Proceedings of the
Annual Stability Conference
Structural Stability Research Council
St. Louis, Missouri, April 2-5, 2019

Design of fixed-base hollow structural section columns subjected to large seismic drift

Hye-eun Kong[1], Matthew R. Eatherton[2], Benjamin W. Schafer[3]

Abstract

During an earthquake, gravity columns in a one-story building must support vertical gravity loads while undergoing large lateral drifts associated with deflections of the vertical seismic force resisting system and deflections of the roof diaphragm. Many of these columns are tube shapes detailed with bases that are cast into the concrete slab or have some amount of fixity, thus creating moments as the top of the column is subjected to lateral drift. While provisions in current building codes require the consideration of lateral drift in conjunction with gravity loads, there is little guidance about how to do this in design. In this paper, three methods for seismic design of gravity columns in one story buildings are discussed: 1) detailing for a pinned base, 2) creating a stable plastic hinge at the base of the column, and 3) designing the column to remain elastic. Slenderness limits for square tube columns are proposed to facilitate the formation of plastic hinges (i.e., option 2). A design procedure is proposed for keeping the tube columns elastic (i.e., option 3) using the interaction equation for axial compression and flexure. It is found that the elastic design procedure is characterized by a simple ratio. An example is presented, demonstrating all three options.

1. Introduction

One-story buildings are a ubiquitous and economical structure for many big box stores, warehouses, factories, and many other uses. Fig. 1 shows a typical building with tilt-up reinforced concrete walls, tube columns, steel beams and joists, and a roof made of wood sheathing or steel deck panels. These types of structures are sometimes referred to as rigid wall / flexible diaphragm (RWFD) buildings and are common throughout the U.S. including high seismic areas (Lawson et al. 2014).

These types of structures may have stiff vertical systems, but flexible diaphragms and the drift at the middle of the diaphragm can be large. Furthermore, studies have shown that code diaphragm loads are too small to keep the diaphragm elastic during design level earthquakes (Rodriguez et al. 2002; 2007). Thus, inelastic diaphragm deflections may lead to additional seismic drift (FEMA 2015).

[1] Graduate Student, Virginia Polytechnic Institute and State University, <hyeeun@vt.edu>
[2] Associate Professor, Virginia Polytechnic Institute and State University, <meather@vt.edu>
[3] Professor, Johns Hopkins University, <schafer@jhu.edu>

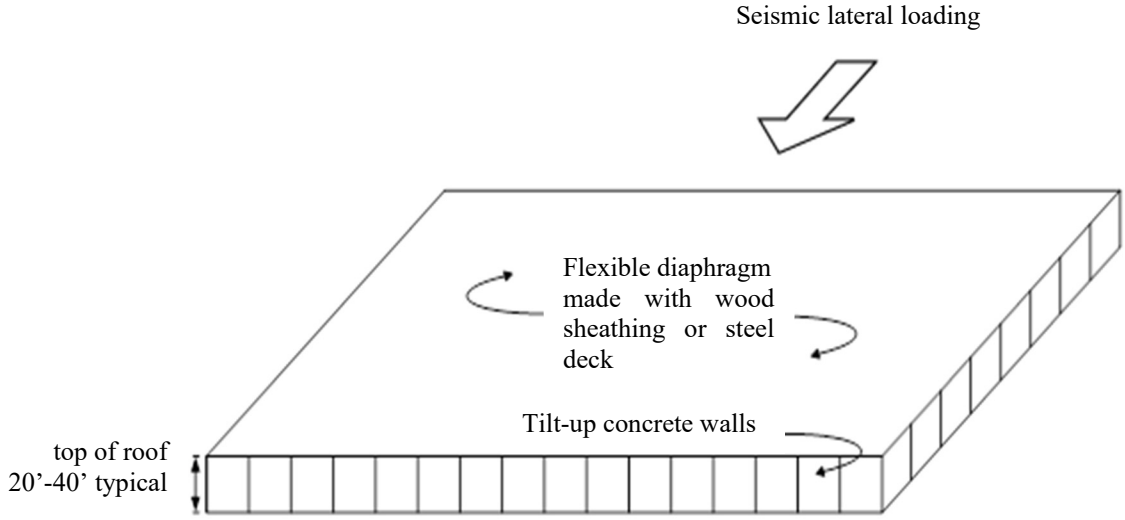

Figure 1: Typical one-story steel building considered

In the 1994 Northridge earthquake, several precast concrete parking garages experienced partial or total collapse in part due to inelasticity in the diaphragm which led to excessive lateral drifts causing the less ductile gravity framing to fail (EERI 1995). Studies have also shown that flexible diaphragms can yield and cause excessive story drifts that dominate structural behavior (Fleischman et al. 1998). From these examples, it is clear that the effect of large lateral drift including elastic and inelastic diaphragm displacements should be considered in the design of the gravity framing. One-story buildings with flexible diaphragms may be vulnerable to similar types of collapse, especially if the diaphragm is allowed to become inelastic and the bases of the columns are fixed.

As shown in Fig. 2, lateral drift at the top of a gravity column is due to deformation of the vertical system (e.g. shear walls), Δ_B, and the deformation of the diaphragm, Δ_D, both of which are made up of elastic and inelastic components. Current U.S. code provisions require the engineer to consider these deformations in the design of the gravity columns. ASCE 7-16 Section 12.12.2 requires that the diaphragm deflection shall not exceed that which will cause attached elements to lose their structural integrity and support the prescribed loads. This could be interpreted to require diaphragm deflections to be limited to that which causes the gravity framing to fail. ASCE 7-16 Section 12.12.5 is more explicit for Seismic Design Categories D through F for which every structural component not part of the seismic force-resisting system shall be designed to support gravity loads while undergoing the design story drift. However, it is not clear whether the design story drift includes diaphragm deflections (elastic or inelastic). AISC 341-16 Section D3 reiterates that where the applicable building code requires deformation compatibility to be checked, that it should be checked. The associated commentary section gives some guidance about avoiding connections in the gravity system that resist moment.

Even if an engineer wanted to check the gravity system for stability when subjected to the total drift considering both elastic and inelastic diaphragm deflections, it may not be clear how to compute inelastic diaphragm drift or how to check the column for stability when subjected to this drift. ASCE 7-16 Section 12.10.3 describes an alternative diaphragm design procedure which better captures the actual seismic diaphragm demands than the conventional procedure and

explicitly accounts for diaphragm inelasticity, but the procedure does not include the estimation of inelastic diaphragm deflections. Recent work on rigid wall flexible diaphragm buildings (FEMA 2015) gives guidance on inelastic diaphragm deflections and recommends a diaphragm deflection amplification factor equal to the response modification factor for the diaphragm which is given in that document as $C_{d\ diaph}$=4.5.

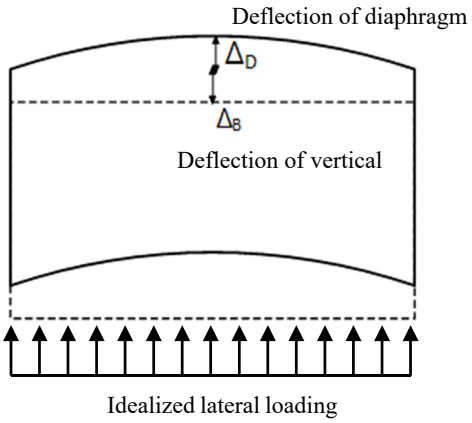

Figure 2: Drifts along the diaphragm span

Detailing of the column in tilt-up buildings can vary, but one approach is shown in Fig. 3. The base of the steel column is often supported directly on the spread footings and sometimes the column base is embedded in the concrete slab on grade. If this type of detailing is used, the concrete slab has the effect of rotationally fixing the base of the column. At the top of the column, joists and joist girders can be installed in a way (the bottom chord can slide on the stabilizer plate) that does not restrain rotation and thus is typically considered pinned (See Fig. 3a). For column axial compression strength, the base fixity has the effect of reducing the effective length and increasing the flexural buckling strength (See top of Fig. 3b). When subjected to lateral drift, shown in the bottom of Fig. 3b as a drift ratio, γ, multiplied by the height of the column, L, then moments develop at the base of the column.

The column must be able to continue supporting gravity load while undergoing this lateral drift. Three options for ensuring column stability during large seismic lateral drift are identified and investigated in this paper:

1. The base of the column may be detailed as a pinned base. This may require compressible material around the column base, or detailing the concrete slab to break during an earthquake. The ability of the base plate to rotate without creating significant moments in the column should be verified by either calculations, models, or tests.
2. A plastic hinge may form at the base of the column. The plastic hinge must be stable such that the column can continue to support the gravity load while undergoing large rotations. Compactness limits have been previously proposed for wide-flange columns for special moment resisting frames to create plastic hinges while supporting large axial loads. A similar approach is taken in this paper for tube columns and a compactness limit is proposed based on data available in the literature.

3. The column can be designed to remain elastic for the combined axial force and moment created by lateral drift and the fixed base boundary condition. A design procedure is proposed and found to be a function of a single nondimensional parameter.

Options 2 and 3, as listed above, are investigated in detail in the following two sections. Then a design example is presented that demonstrates the calculation of lateral drift considering elastic and inelastic diaphragm deflections, and the gravity column is designed for all three options.

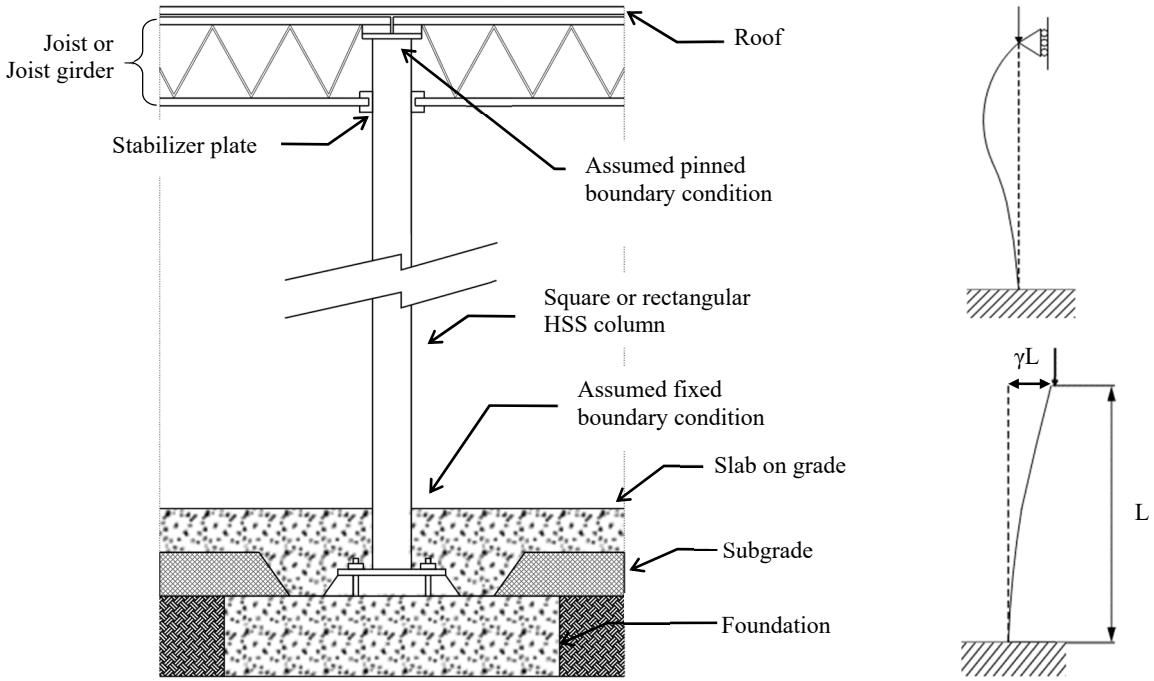

(a) Interior columns (b) Idealized boundary conditions for compression strength

Figure 3: Typical column detailing and fixity

2. Designing Gravity Columns to Plastic Hinge at the Base

Testing on beam-columns subjected to both axial load and lateral drift provide useful information about whether a column can develop a plastic hinge and still support axial load. Since there has been more testing and evaluation of wide flange shapes, this section will begin with a brief review of previous testing on wide flange beam-columns and the resulting development of highly ductile slenderness limits. Then, the previous testing on tube shape beam-columns will be discussed and a highly ductile slenderness limit will be developed based on information available in the literature.

In the past two decades there have been several testing programs subjecting wide flange shapes to both axial force and lateral drift (i.e., moment). Newell and Uang (2006) tested ten W14 columns; Ozkula et al. (2017) tested twenty-five W24 columns; Elkady and Lignos (2016) tested ten W24 columns; Lignos et al. (2016) conducted twelve tests on W14 and W16 columns. Tests on very compact W14 sections with axial loads as large as 0.75 times the axial yield load (P/P_y=0.75) showed that they are capable of large drift (0.07 to 0.09 rad.) without losing axial force resistance (e.g. Newell and Uang 2006). However, W24 columns that had larger web slenderness (but still satisfied the highly ductile limits in AISC 341) exhibited significant local buckling and axial shortening such that these specimens (when subjected to strong axis bending) were not able to

reach 0.03 rad. plastic rotation unless the axial load was very small (0.2 times the axial yield load or P/P_y=0.2) (e.g. Ozkula et al. 2017). Through these testing programs it was found that the ability of a wide flange column to form a stable plastic hinge and continue to support axial force is strongly related to the web slenderness.

Building on these results, researchers have used parametric finite element studies to develop design rules for wide flange columns. Fogarty and El-Tawil (2016) defined a critical axial load ratio (P/P_y) based on when a column was no longer able to support the axial force at a story drift of 0.04 rad. Based on multivariate regression, the expression was found to be a function of the web slenderness and column slenderness as given in Eq. (1). Wu et al. (2018) takes a similar approach, but simplifies and reformulates the equation into a web slenderness limit as given in Eq. (2). Note that this equation is described in Wu et al. (2018) as applying to interior columns which implies a constant axial force, whereas other equations are given for exterior columns for which axial force varies. In both of these studies, axial shortening was not used as a limit and shortening of 2% or more was observed in the models at the target story drift of 0.04 rad. Other studies suggest that the criteria for column slenderness should be based on a limit on column axial shortening (more conservative) rather than the failure to support the specified axial force (Lignos et al. 2016, Ozkula et al. 2017).

$$\frac{\mathrm{P}}{\mathrm{P}_y} \leq 2.6224 - 0.2037 \log\left(\frac{h}{t_w}\right) - 0.3734 \log\left(\frac{L}{r_y}\right) \qquad \text{(Wide-Flange Columns)} \qquad (1)$$

$$\frac{h}{t_w} \leq 9.86 \sqrt{\frac{E}{R_y F_y}} \left(0.72 - \frac{P}{P_y}\right) - 0.62 \frac{L}{r_y} \qquad \text{(Wide-Flange Columns)} \qquad (2)$$

Where P is the applied axial load, P_y is the axial squash load (F_yA), L is the column length, F_y is the yield stress, R_y is the expected yield stress factor from AISC 341, and h, t_w, r_y, and A are section properties: web height, web thickness, minor axis radius of gyration, and area, respectively.

There are significantly less testing programs and finite element studies on tube columns subjected to axial force and lateral drift. Lignos and Krawinkler (2012) identified 71 related tests on tube columns, all conducted in Japan and published exclusively in Japanese except for one study conducted by Kurata et al. (2005). Based on the full set of 71 tests with a range of slenderness ($15 \leq B/t \leq 60$), axial force ratio ($0 \leq P/P_y \leq 0.6$), and yield stress (40 ksi$\leq F_y \leq$72.5 ksi), Lignos and Krawinkler (2012) used multivariate regression to develop a hysteretic model including a prediction equation for plastic rotation at peak moment, θ_p, given by Eq. (3). In this equation, c is a unit conversion factor equal to 6.895 if the yield stress, F_y is used in ksi, and B is the width of the tube.

$$\theta_p = 0.614 \left(\frac{B}{t}\right)^{-1.05} \left(1 - \frac{P}{P_y}\right)^{1.18} \left(\frac{c \cdot F_y}{380}\right)^{-0.11} \qquad \text{(Tube Columns)} \qquad (3)$$

Eq. (3) can be reformulated as a slenderness limit. First, a criterion for column acceptability is assumed based on the peak moment occurring at a plastic rotation equal to 0.02 rad. This choice is based on the assumption that typical bare steel moment connection tests reach their maximum moment at approximately 0.03 rad. before local buckling causes significant reduction in moment

strength and the elastic rotation is approximately 0.01 rad. Substituting θ_p=0.02 in Eq. 3, and assuming a typical R_y=1.1 and modulus of elasticity, E=29,000 ksi and rearranging as a slenderness limit produces Eq. (4). As shown on the right side of Eq. (4), it is proposed that the slenderness limit for the tube not be less than the current highly ductile slenderness limit in AISC 341-16.

$$\frac{\mathrm{B}}{\mathrm{t}} \leq \left[13.7\left(1-\frac{P}{P_y}\right)^{1.124}\left(\frac{E}{R_yF_y}\right)^{0.105} \leq 0.65\sqrt{\frac{E}{R_yF_y}}\right] \qquad \text{(Tube Columns)} \qquad (4)$$

Fig. 4 shows a comparison of existing width to thickness ratio limits in AISC 341-16 and the proposed limits that allow a plastic hinge to form while still supporting axial load. The horizontal axis in Fig. 5 is the axial load ratio, C_a=P/P_y. It is seen that the highly ductile slenderness limit for wide flange shapes proposed by Wu et al. (2018), limits the axial load ratio to a maximum of 0.5 and is more conservative than the existing highly ductile slenderness limits for axial load ratios greater than 0.3. The slenderness limit for tubes proposed in Eq. (4) is shown to be more conservative than the current highly ductile slenderness limit for axial load ratios greater than 0.4 and the slenderness limits approach zero as the axial load ratio approaches 1.0.

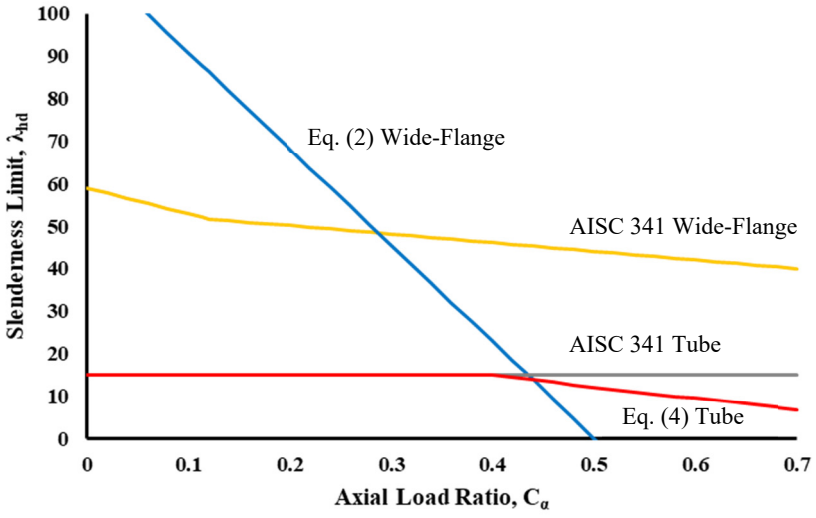

Figure 4: Comparison of slenderness limits

3. Designing Gravity Columns to Stay Elastic

Another approach for design of fixed-base gravity columns for seismic lateral drift is to design the column to stay elastic for the combination of axial compression and flexure. The axial-flexure interaction equation from AISC 360-16 is used as given below in a form that is simplified to consider flexure about one axis only.

$$\frac{P_u}{P_n}+\frac{8}{9}\left(\frac{M_u}{M_n}\right) \leq 1.0, \quad for\ \frac{P_u}{P_n} \geq 0.2 \qquad (5a)$$

$$\frac{1}{2}\frac{P_u}{P_n}+\left(\frac{M_u}{M_n}\right) \leq 1.0, \quad for\ \frac{P_u}{P_n} < 0.2 \qquad (5b)$$

The axial compression strength, P_n, is computed per AISC 360-16 Chapter E, and the flexural strength, M_n is determined according to AISC 360-16 Chapter F. Lateral-torsional buckling (LTB) was not considered because it does not occur in square tube shapes, but flange local buckling was considered in the calculation of moment strength. For compression, the boundary conditions are assumed fixed base and pinned at the top with effective length factor, K=0.8.

Two parameters are introduced to characterize the lateral displacement at the top of the column and the magnitude of the axial load. As shown graphically in Fig. 3b and described by Eq. (6), the displacement at the top of the column is characterized by the story drift ratio, γ, multiplied by the height of the column and the lateral drift is made up components due to deformation of the vertical system (e.g. shear walls), Δ_B, and the deformation of the diaphragm, Δ_D. The magnitude of the axial load is expressed as a normalized ratio of the factored axial compression force, P_u, to the design strength, ϕP_n, as given in Eq. (7). The moment demand can then be calculated as the axial force multiplied by the lateral displacement at the top of the column as given in Eq. (8).

$$\text{Story drift ratio}(\gamma) = \frac{\Delta}{h}, \quad \Delta = \Delta_B + \Delta_D \tag{6}$$

$$\alpha = \frac{P_u}{\phi P_n} \tag{7}$$

$$M_u = P_u(\gamma\, h) = \alpha(\phi\, P_n)(\gamma\, h) \tag{8}$$

Substituting Eq. (7) and Eq. (8) into Eq. (5a) results in Eq. (9). It is assumed that gravity columns will have an axial force that is greater than 0.2 times the axial strength, so Eq. (5b) is not used. Eq. (9) can then be rearranged as given in Eq. (10) as a limit on the axial force ratio, α, given a lateral drift, γ. It is shown that the limit on axial force is characterized by a single member specific parameter, P_nh/M_n. Alternatively, Eq. (10) could be used to find the maximum drift a column can undergo and still satisfy the interaction equation if the axial force is specified.

$$\alpha + \frac{8}{9}\left(\alpha\, \gamma\, \frac{P_n h}{M_n}\right) \leq 1.0 \tag{9}$$

$$\alpha \leq \frac{1}{1+\frac{8}{9}\gamma \frac{P_n\, h}{M_n}} \tag{10}$$

The use of Eq. (10) as a design tool is demonstrated by evaluating six square tube columns with properties given in Table 1. The value of the interaction equation, Eq. (5a) is plotted in Fig. 5 for these six tubes with axial load ratio, α, equal to 0.5, 0.6, 0.7, and 0.8. The following observations are made:

1. Fig. 5 shows that tubes with the same outside dimensions that are thinner have a higher value of the interaction equation. The value of the parameter P_nh/M_n, is larger for thinner sections making them more prone to failure when subjected to lateral drift.
2. The outside dimensions of a tube are not an effective indicator of the maximum lateral drift a column can sustain before the interaction equation is violated. As shown in Figure 5, the different tube sizes are interspersed.
3. The parameter, P_nh/M_n, is shown to be effective at predicting whether a section is more or less vulnerable to reaching the interaction limit state as lateral drift is increased.

Table 1: Section properties for the 6 square HSS columns used as an example

	HSS 4x4x$^1/_2$	HSS 4x4x$^1/_8$	HSS 8x8x$^5/_8$	HSS 8x8x$^1/_8$	HSS 12x12x$^3/_4$	HSS 12x12x$^3/_{16}$
r_y (in)	1.41	1.58	2.99	3.21	4.56	4.82
P_n/P_y	0.12	0.15	0.51	0.43	0.75	0.52
P_nh/M_n	33.9	41.5	67.0	84.3	64.2	69.1

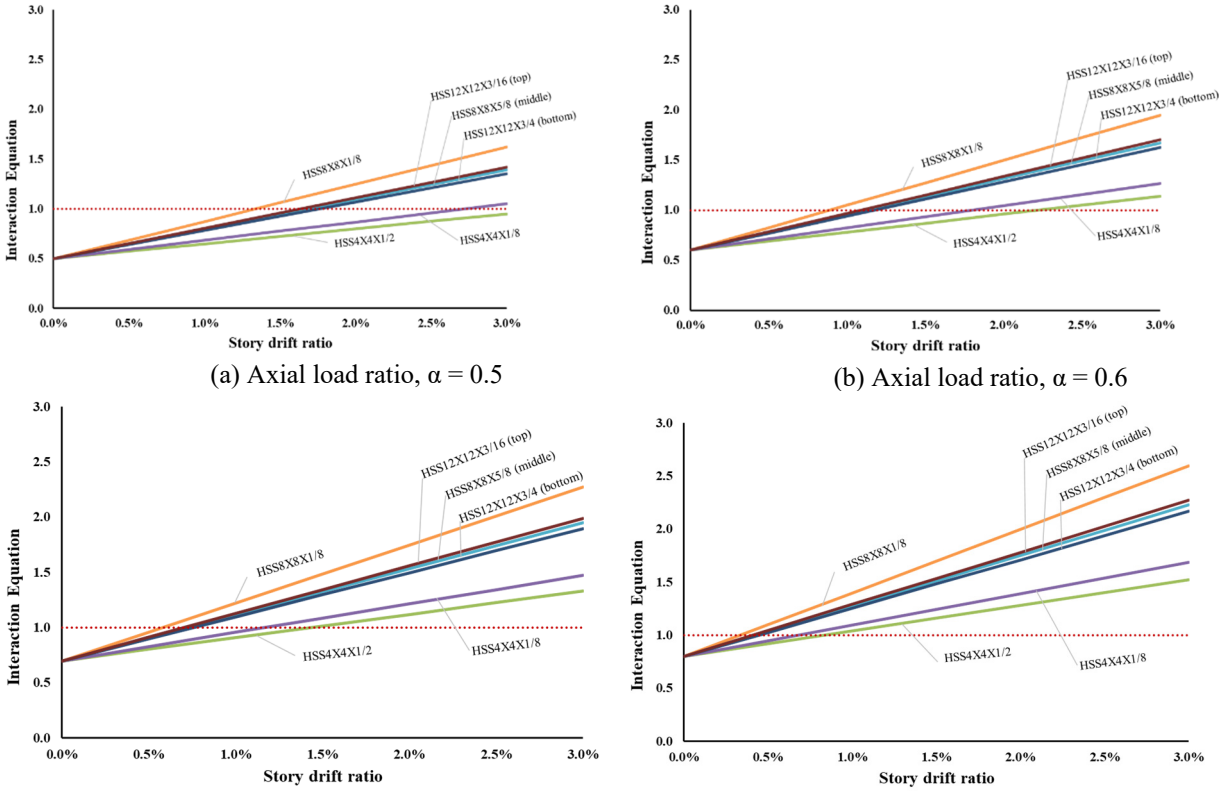

(a) Axial load ratio, α = 0.5

(b) Axial load ratio, α = 0.6

(c) Axial load ratio, α = 0.7

(d) Axial load ratio, α = 0.8

Figure 5: Evaluating maximum allowable lateral drift for six example tube column sections

Based on these results, a simple design procedure can be used to determine the maximum allowable lateral drift for a tube gravity column. First, it is necessary to calculate the value of P_nh/M_n, for the trial column size. To make this easier, values of P_nh/M_n, are given in Table 2 for all square HSS shapes in the AISC manual. Then either Eq. (10) or the design charts given in Fig. 6 can be used to determine whether the axial load ratio, α, is adequate for the amount of drift, γ, that is expected. This will likely be an iterative process.

Table 2: Values for the parameter $\frac{P_n h}{M_n}$ for all square HSS columns

Section	P_nh/M_n	Section	P_nh/M_n	Section	P_nh/M_n
HSS2X2X$^1/_8$	18.15	HSS5X5X$^3/_8$	44.42	HSS10X10X$^1/_4$	84.49
HSS2X2X$^3/_{16}$	17.48	HSS5X5X$^1/_2$	43.42	HSS10X10X$^5/_{16}$	74.21
HSS2X2X$^1/_4$	16.92	HSS5-$^1/_2$X5-$^1/_2$X$^1/_8$	68.63	HSS10X10X$^3/_8$	67.85
HSS2-$^1/_4$X2-$^1/_4$X$^1/_8$	20.55	HSS5-$^1/_2$X5-$^1/_2$X$^3/_{16}$	53.13	HSS10X10X$^1/_2$	67.90
HSS2-$^1/_4$X2-$^1/_4$X$^3/_{16}$	20.01	HSS5-$^1/_2$X5-$^1/_2$X$^1/_4$	50.59	HSS10X10X$^5/_8$	67.86
HSS2-$^1/_4$X2-$^1/_4$X$^1/_4$	19.24	HSS5-$^1/_2$X5-$^1/_2$X$^5/_{16}$	50.22	HSS10X10X$^3/_4$	68.21
HSS2-$^1/_2$X2-$^1/_2$X$^1/_8$	22.93	HSS5-$^1/_2$X5-$^1/_2$X$^3/_8$	49.51	HSS12X12X$^3/_{16}$	69.13
HSS2-$^1/_2$X2-$^1/_2$X$^3/_{16}$	22.32	HSS6X6X$^1/_8$	78.15	HSS12X12X$^1/_4$	74.40
HSS2-$^1/_2$X2-$^1/_2$X$^1/_4$	21.71	HSS6X6X$^3/_{16}$	62.29	HSS12X12X$^5/_{16}$	77.25
HSS2-$^1/_2$X2-$^1/_2$X$^5/_{16}$	21.09	HSS6X6X$^1/_4$	55.82	HSS12X12X$^3/_8$	69.89
HSS3X3X$^1/_8$	27.70	HSS6X6X$^5/_{16}$	54.97	HSS12X12X$^1/_2$	63.66
HSS3X3X$^3/_{16}$	27.17	HSS6X6X$^3/_8$	54.34	HSS12X12X$^5/_8$	63.89
HSS3X3X$^1/_4$	26.41	HSS6X6X$^1/_2$	53.30	HSS12X12X$^3/_4$	64.16
HSS3X3X$^5/_{16}$	25.77	HSS6X6X$^5/_8$	51.74	HSS14X14X$^5/_{16}$	67.57
HSS3X3X$^3/_8$	25.54	HSS7X7X$^1/_8$	88.58	HSS14X14X$^3/_8$	70.42
HSS3-$^1/_2$X3-$^1/_2$X$^1/_8$	32.78	HSS7X7X$^3/_{16}$	77.77	HSS14X14X$^1/_2$	58.55
HSS3-$^1/_2$X3-$^1/_2$X$^3/_{16}$	32.23	HSS7X7X$^1/_4$	64.29	HSS14X14X$^5/_8$	58.85
HSS3-$^1/_2$X3-$^1/_2$X$^1/_4$	31.57	HSS7X7X$^5/_{16}$	63.69	HSS14X14X$^3/_4$	59.21
HSS3-$^1/_2$X3-$^1/_2$X$^5/_{16}$	30.83	HSS7X7X$^3/_8$	63.20	HSS14X14X$^7/_8$	59.61
HSS3-$^1/_2$X3-$^1/_2$X$^3/_8$	30.17	HSS7X7X$^1/_2$	62.28	HSS16X16X$^5/_{16}$	59.25
HSS4X4X$^1/_8$	41.52	HSS7X7X$^5/_8$	61.22	HSS16X16X$^3/_8$	61.97
HSS4X4X$^3/_{16}$	36.80	HSS8X8X$^1/_8$	84.34	HSS16X16X$^1/_2$	58.74
HSS4X4X$^1/_4$	36.17	HSS8X8X$^3/_{16}$	87.91	HSS16X16X$^5/_8$	53.94
HSS4X4X$^5/_{16}$	35.48	HSS8X8X$^1/_4$	74.14	HSS16X16X$^3/_4$	54.27
HSS4X4X$^3/_8$	35.22	HSS8X8X$^5/_{16}$	67.65	HSS16X16X$^7/_8$	54.55
HSS4X4X$^1/_2$	33.87	HSS8X8X$^3/_8$	67.75	HSS18X18X$^1/_2$	58.19
HSS4-$^1/_2$X4-$^1/_2$X$^1/_8$	50.31	HSS8X8X$^1/_2$	67.24	HSS18X18X$^5/_8$	50.33
HSS4-$^1/_2$X4-$^1/_2$X$^3/_{16}$	41.51	HSS8X8X$^5/_8$	67.02	HSS18X18X$^3/_4$	49.64
HSS4-$^1/_2$X4-$^1/_2$X$^1/_4$	41.32	HSS9X9X$^1/_8$	78.71	HSS18X18X$^7/_8$	49.85
HSS4-$^1/_2$X4-$^1/_2$X$^5/_{16}$	40.54	HSS9X9X$^3/_{16}$	86.67	HSS20X20X$^1/_2$	52.05
HSS4-$^1/_2$X4-$^1/_2$X$^3/_8$	39.83	HSS9X9X$^1/_4$	81.14	HSS20X20X$^5/_8$	49.90
HSS4-$^1/_2$X4-$^1/_2$X$^1/_2$	38.48	HSS9X9X$^5/_{16}$	69.90	HSS20X20X$^3/_4$	45.39
HSS5X5X$^1/_8$	59.43	HSS9X9X$^3/_8$	68.69	HSS20X20X$^7/_8$	45.72
HSS5X5X$^3/_{16}$	46.61	HSS9X9X$^1/_2$	68.37	HSS22X22X$^3/_4$	43.23
HSS5X5X$^1/_4$	45.86	HSS9X9X$^5/_8$	68.57	HSS22X22X$^7/_8$	42.11
HSS5X5X$^5/_{16}$	45.17	HSS10X10X$^3/_{16}$	81.05		

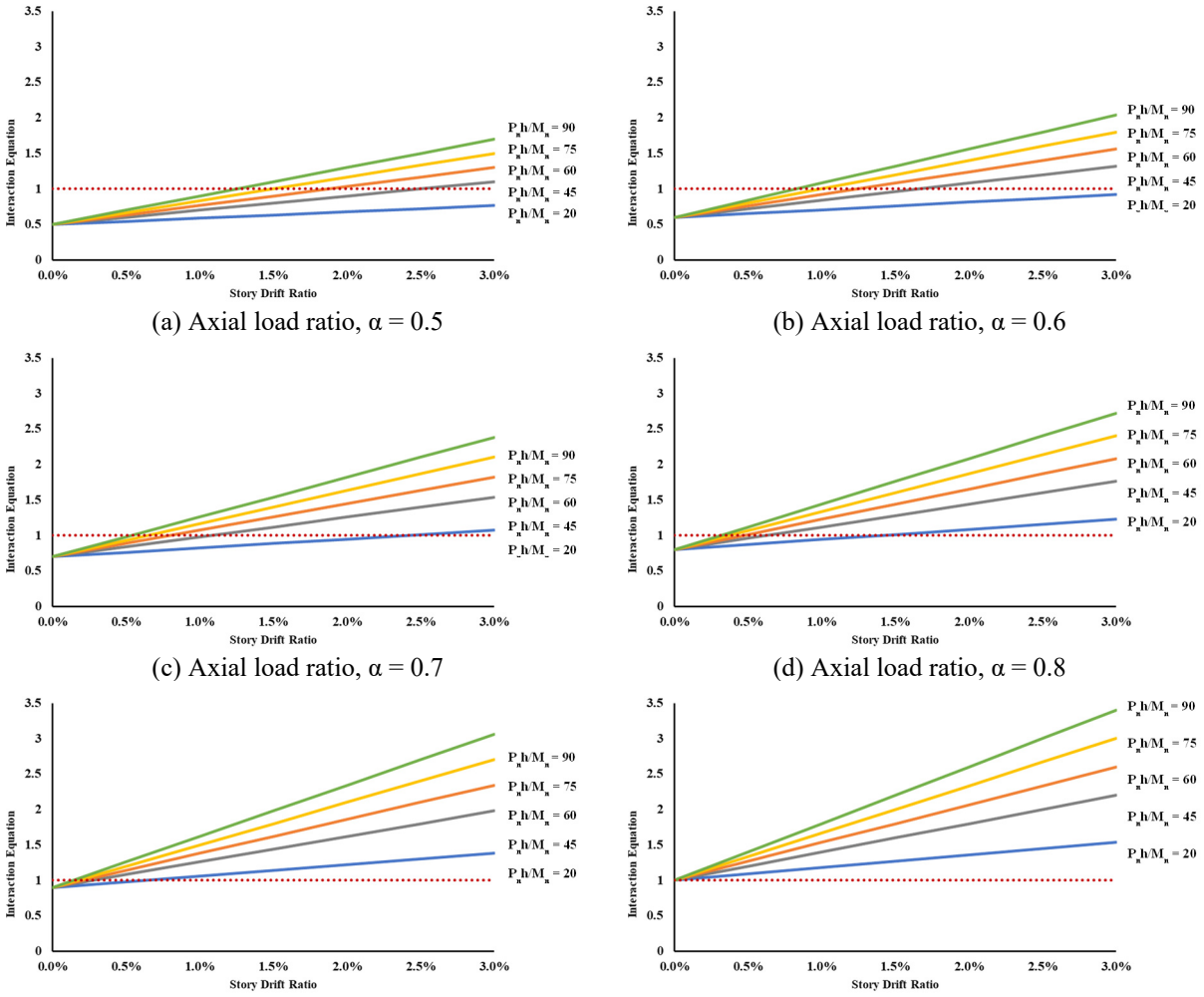

(a) Axial load ratio, α = 0.5

(b) Axial load ratio, α = 0.6

(c) Axial load ratio, α = 0.7

(d) Axial load ratio, α = 0.8

(e) Axial load ratio, α = 0.9

(f) Axial load ratio, α = 1.0

Figure 6: The design charts of HSS columns

4. Design Example Introduction and Drift Calculation

To illustrate the design concepts introduced in this paper, an example building is defined and seismic lateral drift at the top of the gravity columns is calculated. In the next section, a typical gravity column will be designed using all three approaches.

The example building, shown in Fig. 7, is taken from the example in FEMA 1026 (FEMA 2015) with some minor modifications. The building is meant to represent a typical concrete tilt-up wall building with a wood structural panel roof diaphragm. The concrete shear wall is 9.25 in. thick and made out of concrete with 150 pcf unit weight and 4000 psi compressive strength. A "hybrid roof structure" is used which consists of OSB panels on open web steel joists, is used. The roof height is 30 feet above finish floor surface with another 3-foot to the top of parapet. The roof has a 12 psf dead load and 30 psf snow load.

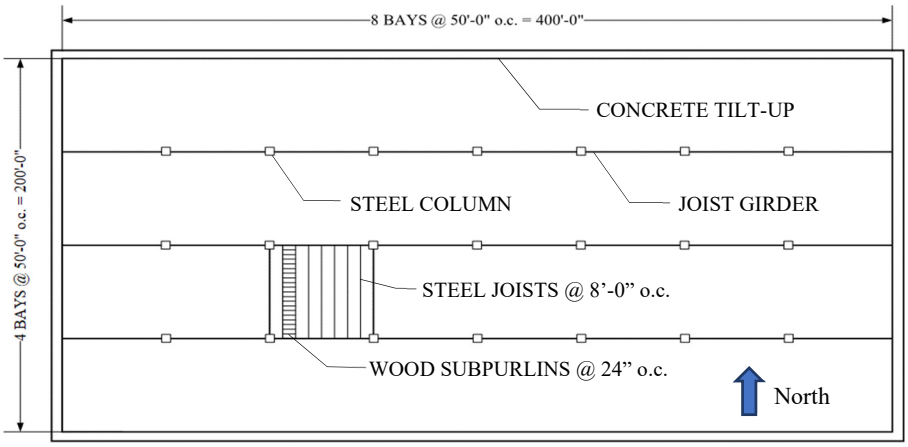

Figure 7: Plan view of the prototype building

The example building is assumed to be located in a high seismic zone with mapped spectral accelerations, S_s=1.5g and S_1=0.6g, and a resulting seismic response coefficient, C_s=0.25, calculated using the provisions of ASCE 7-16. The seismic base shear is found to be 658 kips which is also the total lateral force used in diaphragm design. Based on a linear shear diagram, the diaphragm nailing is scheduled in six zones as summarized in Table 3 and shown in Fig. 8. The chords are L5x5x5x$^3/_8$.

Table 3: Diaphragm nailing schedule

	$^{15}/_{32}$" Structural I OSB Sheathing with 10d nails (0.148" dia. x 2" long minimum)				
Zone	Framing Width at Adjoining Edges	Lines of Nails	Nailing per line at Boundary & Continuous Edges	Nailing per line at Other Edges	ASD Allowable Shear (plf)
1	2x	1	6" o.c.	6" o.c.	320
2	2x	1	4" o.c.	6" o.c.	425
3	2x	1	2½" o.c.	4" o.c.	640
4	3x	1	2" o.c.	3" o.c.	820
5	4x	2	2½" o.c.	4" o.c.	1005
6	4x	2	2½" o.c.	3" o.c.	1290

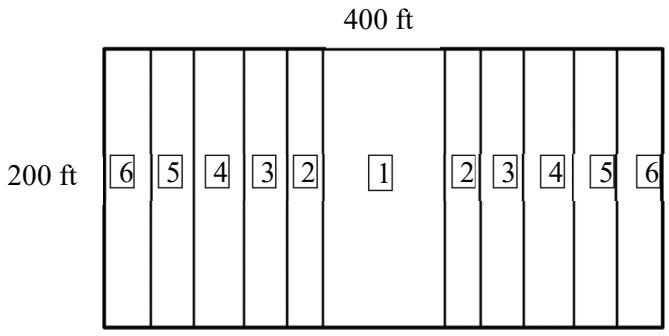

Figure 8: North/South Nailing Zone Layout

The diaphragm deflections will be larger in the north/south direction, so for gravity column design, the drift in the north/south direction is used. It is noted that although the fixed-base gravity columns provide some resistance to lateral drift, that the effect is neglected in these calculations.

Eq. (11) is a method for calculating diaphragm deflection taken from the Special Design Provisions for Wind and Seismic (SDPWS) (AWC 2015).

$$\delta_{dia} = \frac{5vL_{dia}^3}{8EA_{chord}W} + \frac{0.25vL_{dia}}{1000G_a} + \frac{\Sigma(x\Delta_c)}{2W} \quad (11)$$

In Eq. (11), the distributed lateral diaphragm loading is, v = 1644 plf, the diaphragm span is, L_{dia}=400 ft, the diaphragm depth is, W=200 ft, chord modulus of elasticity is, E=29,000 ksi, chord area is, A_{chord}=3.65 in^2, and the diaphragm shear stiffness, G_a, is given in Table 4 (as obtained from SDPWS-2015 Table 4.2A and 4.2B). The chord slip at each connection, Δ_c, is assumed to be zero so the last term in Eq. (11) is neglected.

Table 4: Diaphragm shear deformation

Zone	v_{left} (plf)	v_{right} (plf)	$v_{i.ave}$ (plf)	L_i (ft)	G_a	$\frac{v_{ave}L_i}{1000G_a}$
1	395	0	198	32	24	0.26 in
2	592	395	494	32	15	1.05 in
3	855	592	724	32	20	1.16 in
4	1118	855	987	32	26	1.21 in
5	1381	1118	1250	32	44	0.91 in
6	1644	1381	1513	24	51	0.71 in
					$\sum$ =	5.31 in

The resulting diaphragm deflection is:

$$\delta_{dia} = 2.17\ in. + 5.31\ in. + 0.0\ in. = 7.48\ in. \quad (12)$$

Although the diaphragm deflection will make up the majority of the lateral drift, shear wall deflection should be added to the diaphragm deflection to obtain the total drift. The deflection of a cantilever shear wall has two components, namely a flexural component and a shear component.

$$\delta_{wall} = \delta_{wall.flexure} + \delta_{wall.shear} \quad (13)$$

$$\delta_{wall} = \frac{Ph^3}{3EI} + \frac{1.2Ph}{GA} \quad (14)$$

The seismic load in the diaphragm was calculated with seismic weight that included half of the weight of the concrete walls on the north and south faces of the building (these are leaning on the diaphragm for north-south motions). The load at the top of the either the east or west walls, P=425 kips, is computed as half of the load in the diaphragm, 329 kips, plus additional lateral load due to the seismic weight of the east-west walls, 96 kips. The material properties and section properties of shear wall are computed for the eight 25-ft wide concrete shear walls (9¼ in thick, f'_c = 4000 psi). The height is, h=30 feet, modulus of elasticity is, E=3600 ksi, shear modulus is, G=1500 ksi, total moment of inertia for all eight walls is, I_g=167x10^6 in^4, and area of the eight walls, A_g=22,200 in^2. The resulting wall deflection is:

$$\delta_{wall} = 0.022\ in. + 0.011\ in. = 0.033\ in \quad (15)$$

The computed diaphragm deflection and wall deflection are elastic deformations due to design level loads and are not equal to the expected actual deflections considering inelasticity. For the precast shear walls, the deflection amplification factor, C_d, is given in ASCE 7-16 as 4.0. For the diaphragm, there is no specified deflection amplification factor, $C_{d\text{-}diaph}$. As discussed in the introduction, conventional diaphragm design loads (such as those used in this example) are smaller than the elastic loads and may lead to diaphragm inelasticity. If engineers want to compute diaphragm loads that are expected to produce elastic diaphragm behavior, they should use the alternative diaphragm design procedures in ASCE 7-16 with diaphragm response modification factor, R_s=1.0. Future editions of ASCE 7-16 may also include provisions for rigid wall flexible diaphragm buildings such as this example with explicit specification of a diaphragm deflection amplification factor, $C_{d\text{-}diaph}$. However, without any guidance, the diaphragm deflection amplification factor is taken as $C_{d\text{-}diaph}$=1.0 for this example, which could be unconservative. The total drift at the midspan of the diaphragm is therefore:

$$\delta_M = \frac{C_d \delta_{wall}}{I_e} + \frac{C_{d-diaph} \delta_{dia}}{I_e} = \frac{4.0(0.033\ in)}{1.0} + \frac{1.0(7.48\ in)}{1.0} = 7.61\ in \quad (16)$$

$$\text{Drift ratio, } \gamma = \frac{\delta_M}{h} = \frac{7.61\ in.}{30\ ft(12\ \frac{in.}{ft})} = 0.021 \quad (17)$$

5. Design Example – Gravity Column Design

A typical gravity column at the middle of the building is designed for each of the three options including: 1) detailing for a pinned base, 2) creating a stable plastic hinge at the base of the column, and 3) designing the column to remain elastic. First, the factored axial load is calculated. The roof dead load is given as 12 psf, snow load is 30 psf, and tributary area is 2500 ft^2. The resulting factored axial compression force is:

$$P_u = 156 \text{ kip} \quad (18)$$

5.1 Option 1 - Detail Column for Pinned Base

To create an effective pin at the base of the column, it is necessary to hold the slab back from the base connection, minimize the rotational restraint created by the base plate, evaluate the amount of moment that is generated at the base, and either verify it can be neglected or consider it in column design. Fig. 9 shows a possible base detail. The subgrade is placed over the base plate, so it is not embedded in concrete and compressible material is wrapped around the column before placing the concrete. The thickness of the compressible material can be calculated based on the drift ratio multiplied by the distance from the top of the slab to the column base. The drift ratio was calculated to be 0.021 and if the top of slab is 12 in. above the base plate, then the compressible material should be at least 0.25 in. thick. Compressible material with thickness equal to 0.5 in. is selected.

The column has pinned-pinned boundary conditions, so the design axial strength of the column can be read directly from Table 4-4 in the AISC Manual. An HSS8x8x$^3/_8$ is selected with a design strength, ϕP_n=174 kips for a height of 30 ft which is greater than the required strength of P_u=156 kips.

There are different approaches for designing the base plate connection to have small rotational restraint. One approach is to make the base plate as thin as possible and spread out the anchor bolts as shown in Fig. 9. In this case, the base plate thickness should be calculated based on the necessary area of bearing, not the full base plate area. Regardless of the approach selected, the rotational restraint and resulting moment at the base of the column should be evaluated using calculations, finite element modeling, or tests. If the moment at the base of the column is non-negligible, then axial-flexure interaction should be checked for the column.

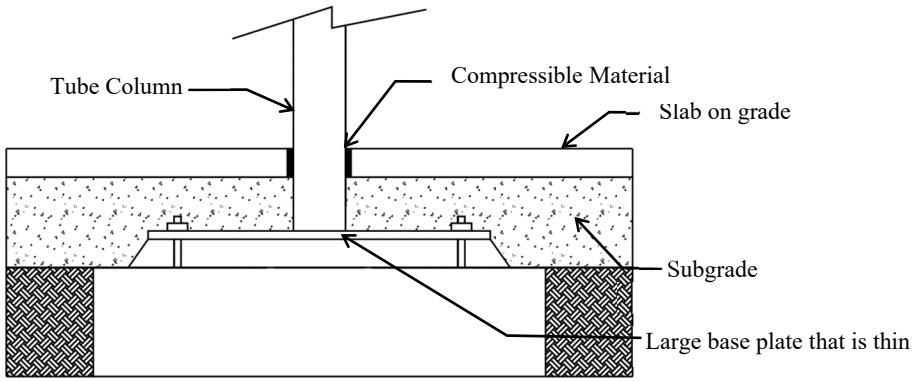

Figure 9: Possible detailing for pinned base

5.2 Option 2 – Design Column for Plastic Hinge at Base

Section 2 of this paper describes how to create a stable plastic hinge by limiting the section slenderness using Eq. (4). Try an HSS8x8x$^1/_2$ and check the compactness limit from Eq. (4):

$$14.2 \leq \left[13.7\left(1-\frac{156\ kip}{(13.5\ in^2)(50\ ksi)}\right)^{1.124}\left(\frac{29000\ ksi}{(1.1)(50\ ksi)}\right)^{0.105} \leq 0.65\sqrt{\frac{29000\ ksi}{(1.1)(50\ ksi)}}\right]$$

$$14.2 \leq 14.9 \qquad \therefore \text{O.K.} \tag{19}$$

Also, it is necessary to check if the column design axial strength is greater than the required axial strength. In this case, even though the base is assumed to be initially fixed, after the plastic hinge forms the base is effectively pinned and therefore the effective length is equal to the height of 30 ft. From Table 4-4 in the AISC Manual, the design strength is found to be, ϕP_n=217 kips, which is greater than the required strength of P_u=156 kips.

5.3 Option 3 – Design Column to Remain Elastic

The story drift was computed in Section 4 to be 2.1%. The procedure described in Section 3 will be applied to design the gravity column to stay elastic for this amount of drift. For this example, start by assuming P_nh/M_n = 75 and the allowable axial load ratio can be calculated using Eq. (10) to be:

$$\alpha_{max} = \frac{1}{1+\frac{8}{9}\gamma\frac{P_nh}{M_n}} = \frac{1}{1+\frac{8}{9}(0.021)(75)} = 0.42 \quad \text{preliminary} \tag{20}$$

Find a column that has design axial strength equal to 156 kips / 0.42 = 371 kips with effective length, 0.8(30 ft) = 24 ft. An HSS10x10x3/8 is selected with design axial strength equal to

ϕP_n=400 kips. The actual axial load ratio is 156/400=0.39 and the value of P_nh/M_n = 67.85 can be found in Table 2. With these final values, it is verified that the axial load ratio is less than the maximum:

$$0.39 \leq \frac{1}{1+\frac{8}{9}\gamma\frac{P_nh}{M_n}} = \frac{1}{1+\frac{8}{9}(0.021)(67.85)} \quad (21)$$

$$0.39 \leq 0.44 \qquad \therefore \text{O.K.} \quad (22)$$

The HSS10x10x$^3/_8$ is thus shown to be adequate. It is noted that this column design is based on a gravity column in the middle of the diaprhagm where the maximum deflection occurs. The drift is smaller near the walls and thus it is possible to design smaller columns near the edges of the diaprhagm span.

6. Conclusions

Fixed base columns in one-story buildings subjected to large lateral seismic drift may be prone to failure during earthquakes unless they are properly designed and detailed. Although current U.S. building codes require that seismic lateral drift be considered in the stability of elements like these columns, there is little guidance on how to design the columns to accommodate drift. In this paper, three options are identified and explored for the design of these gravity columns, which are:

1. Detail the base of the column to minimize rotational fixity. The concrete slab should not be cast around the base plate, and compressible material should be placed between the slab and the column. The base plate should be detailed to minimize the rotational restraint which should be evaluated through analysis or experiments.
2. Design the column to develop a plastic hinge at the base. A compactness limit for the tube wall is proposed based on information found in the literature.
3. Design the column to remain elastic for the combination of axial force and moment associated with lateral drift. A design procedure is developed which is based on a single parameter.

A design example was presented to demonstrate all three design examples. Based on the design example and the examination of the design approaches, two observations are made:

1. In one-story buildings with flexible diaphragms, the diaphragm deflection can dominate the drift. Based on building collapses during Northridge and follow-up studies, there is reason to believe diaphragms designed to current building codes may experience inelastic deformations. In some cases, it may be appropriate to apply a diaphragm deflection amplification factor to account for inelasticity.
2. Detailing the column to have a pinned base resulted in the lightest column for the example building, but requires special consideration and detailing. Designing the column to develop a plastic hinge favors columns with thicker walls, and conversely designing the column to remain elastic leads to larger columns with thinner walls

Acknowledgments

This work was part of the Steel Diaphragm Innovation Initiative (SDII) which is funded by AISI, AISC, SDI, SJI, and MBMA and is part of the Cold-Formed Steel Research Consortium (CFSRC).

References

AISC 360 (2016). “Specification for Structural Steel Buildings.” ANSI/AISC-360-16, American Institute of Steel Construction, Chicago, IL.

AISC 341 (2016). “Seismic Provisions for Structural Steel Buildings.” ANSI/AISC-341-16, American Institute of Steel Construction, Chicago, IL.

ASCE 7 (2016). “Minimum Design Loads and Associated Criteria for Buildings and Other Structures.” American Society of Civil Engineers, Reston, VA.

AWC (2015). “Special Design Provisions for Wind and Seismic (SDPWS).” American Wood Council, Leesburg, VA.

Elkady, A. and Lignos, D. G. (2016). “Dynamic Stability of Deep and Slender Wide-Flange Steel Columns – Full Scale Experiments.” *Proceeding of the Annual Stability Conference Structural Stability Research Council*, Florida.

Forgarty, J. and El-Tawil, S. (2016). “Collapse Resistance of Steel Columns under Combined Axial and Lateral Loading.” *Journal of Structural Engineering*, 142 (1), 04015091.

Fadden, M. F. (2013). “Cyclic Bending Behavior of Hollow Structural Sections and their Application in Seismic Moment Frame Systems.” *(Dissertation)*, Dep. of Civil and Environmental Engineering, University of Michigan.

FEMA (2015). “Seismic Design of Rigid Wall-Flexible Diaphragm Buildings: An Alternate Procedure.” *Report FEMA P-1026*, Federal Emergency Management Agency, Washington, DC.

Fleischman, R. B. et al. (1998). “Seismic Behavior of Precast Parking Structure Diaphragms.”, *PCI Journal*, 43(1), 38-53.

Hall, J., & Earthquake Engineering Research Institute. (1995). “Northridge earthquake of January 17, 1994: Reconnaissance Report (Vol. 1).” Oakland, Calif.: Earthquake Engineering Research Institute.

Kurata, M., & Nakashima, M., & Suita, K. (2005). “Effect of Column Base Behavior on the Seismic Response of Steel Moment Frames.” *Journal of Earthquake Engineering*, 9 (2) 415-438.

Lawson, J., & Kelly, D. J., & Koliou, M., & Filiatrault, A. (2014). “Development of Seismic Design Methodologies for Rigid Wall-Flexible Diaphragm Structures.” *Proceedings of the Tenth U.S. National Conference on Earthquake Engineering*, Anchorage, Alaska.

Lignos, D. G., & Cravero, J., & Elkady, A. (2016). “Experimental Investigation of the Hysteretic Behavior of Wild-Flange Steel Columns under High Axial Load and Lateral Drift Demands.” *Proceeding of 11th Pacific Structural Steel Conference*, Shanghai, China.

Lignos, D., & Krawinkler, H. (2012). “Sidesway Collapse of Deteriorating Structural Systems under Seismic Excitations.” *(Dissertation)*, Dep. of Civil and Environmental Engineering, Stanford University.

Naeim, F. (2012). “The Seismic Design Handbook.” Springer Science & Business Media.

Newell, J. D., & Uang, C. M. (2006). “Cyclic Behavior of Steel Columns with Combined High axial Load and Drift Demand.” (*Report No. SSRP-06/22*), Dep. of Structural Engineering, University of California.

Newell, J. D., & Uang, C. M. (2008). “Cyclic Behavior of Steel Side-Flange Columns Subjected to Large Drift.” *Journal of Structural Engineering*, 134 (8), 1334-1342.

Ozkula, G., & Harris, J., & Uang, C. M. (2017). “Observations from Cyclic Tests on Deep, Wide-Flange Beam-Columns.” *Engineering Journal*, 45-59.

Rodriguez, M. E., & Restrepo, J. I., & Carr, A. J. (2002). “Earthquake-Induced Floor Horizontal Accelerations in Buildings.” *Earthquake Engineering & Structural Dynamics*, 31, 693-718.

Rodriguez, M. E., & Restrepo, J. I., & Blandón, J. J. (2007). “Seismic design forces for rigid floor diaphragms in precast concrete building structures.” *Journal of Structural Engineering*, 133 (11), 1604-1615.

Qayyum, B. (2017). “Computational Modeling of One-Story Building with Nonlinear Steel Deck Diaphragms Subjected to Earthquakes.” (*Report No. 1562669*). Alexandria, Virginia: National Science Foundation.

Uang, C. M., & Ozkula, G., & Harris, J. (2015). “Observations from Cyclic Tests on Deep, Slender Wide-Flange Structural Steel Beam-Column Members." *Proceedings of the Annual Stability Conference Structural Stability Research Council*, Tennessee, Nashville., 247–263.

Wu, T. Y., & El-Tawil, S., & McCormick, J. (2018a). “Seismic Collapse Response of Steel Moment Frames with Deep Columns.” *Journal of Structural Engineering*, 144 (9), 04018145.

Wu, T. Y., & El-Tawil, S., & McCormick, J. (2018b). “Highly Ductile Limits for Deep Steel Columns.” *Journal of Structural Engineering*, 144 (4), 04018016.